V. ELECTRODYNAMICS OF MEDIA[*]

Academic and Research Staff

Prof. L. J. Chu   Prof. J. I. Glaser   L. Frenkel
Prof. H. A. Haus   Prof. P. Penfield, Jr.   R. H. Rines

Graduate Students

B. L. Diamond   P. W. Hoff   A. C. Nelson
H. Granek   E. R. Kellet, Jr.   C. M. Watson

A. EFFECT OF CROSS RELAXATION ON LAMB DIP

The Lamb dip[1] provides a means for determining parameters of the lasing medium, or can be used for frequency stabilization of a laser. Extensive studies have been done on the Lamb dip in the He-Ne system, particularly at the 1.15 transition.[2] Some work has been accomplished in the water-vapor laser[3] and in the CO_2 laser.[4] In CO_2 it was found that the Lamb dip appeared only under surprisingly low pressures.

The differences between a CO_2 laser and an He-Ne laser can easily explain the difficulty in obtaining a Lamb dip in a CO_2 laser. The extremely long lifetime of the upper level in CO_2 permits a diffusion of molecules from one velocity group to another within the Doppler line, thereby making it difficult to burn a hole in the Doppler line at any one frequency. This mechanism, recognized as a possibility by Bennett,[5] is called cross relaxation and tends to make an inhomogeneously broadened system behave more like a homogeneously broadened one. This effect becomes pronounced in CO_2 because the collisions that tend to shift excited molecules between velocity classes, that is, small angle grazing collisions or relaxation to and from different rotational levels, all take place in times shorter than the relaxation rate of the upper level of the laser. This is not the case in an He-Ne laser.

Comparing two physical situations, one with cross relaxation within the Doppler line, the other without, while assuming that the homogeneous and inhomogeneous contributions to the line width are the same in both cases, we find that in the case with cross relaxation the depth of the hole burned by the laser radiation is smaller and the whole Doppler-broadened line is pulled down by it.

Figure V-1, shows the effects of hole burning in a travelling-wave laser in various limits of cross relaxation. In Fig. V-1a there is no cross relaxation, and a hole is burned only around the frequency of operation. In Fig. V-1b there is some finite cross relaxation, and a hole is burned while the hole line is pulled down also. In Fig. V-1c the cross relaxation is very strong, and the diffusion into the velocity group of the hole

burning becomes large enough to prevent a hole from being burned. This case behaves like a homogeneously broadened line even though it is inhomogeneously broadened. Note there would be no Lamb dip in this case.
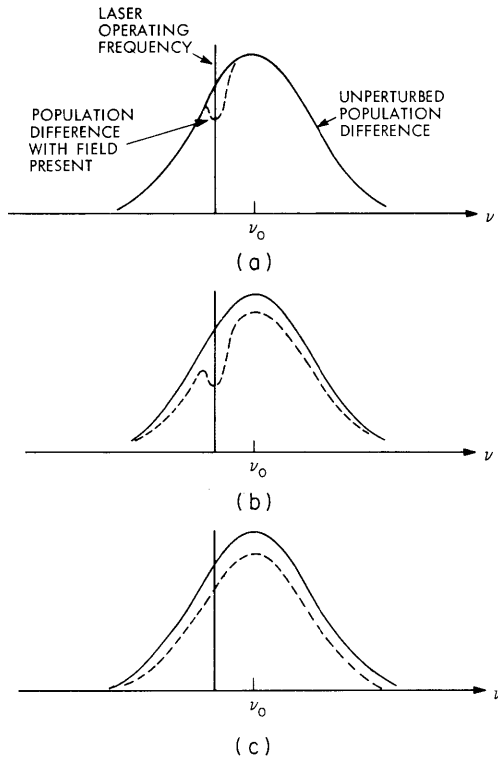

Fig. V-1.

Effect of hole burning in a traveling-wave laser. (a) No cross relaxation. (b) Finite cross relaxation. (c) Strong cross relaxation.

We now proceed to include cross relaxation in the Szöke-Javan theory of Lamb dip.

The intensity, I, of an optical electrical field, E, of propagation constant k is given by

$$I = \frac{cE^2}{8\pi}$$

(1)

which gives the spatial rate of growth of the intensity I. The gain constant can be expressed in terms of the cross section $\sigma(v, k, \omega)$ of the velocity group $v, v + dv$ to an optical field of propagation constant k and frequency ω. Denoting the inversion of a particular velocity group $v, v + dv$ by $n(v)\, dv$, we have for the gain constant[2] of a wave with propagation constant k

$$\alpha = \int_{-\infty}^{\infty} n(v)\, \sigma(v, k, \omega)\, dv.$$

(2)

The population inversion $n(v)$ is affected by the presence of the laser field. We describe

the inversion by the rate equation.

$$\frac{\partial n}{\partial t} = -\gamma(v)\, n(v) - \int \Gamma(v',v)\, n(v)\, dv' + \int \Gamma(v,v')\, n(v')\, dv'$$

$$+ R(v) - \sum_{k,\omega} \frac{2}{\hbar\omega}\, n(v)\, \sigma(v,k,\omega)\, E^2(k,\omega)\, \frac{c}{8\pi}.$$ (3)

The first term represents the relaxation into levels other than the ones considered. The second term is the loss of inverted particles through cross relaxation into the velocity group $v', v' + dv'$. The third term is the reverse process when particles in the velocity group $v', v + dv'$ relax into the group $v, v+ dv$. The term R(v) represents the pump, and the last term is the depletion of inversion caused by the presence of the laser field. The summation over k and ω is included (see Szöke and Javan[2]) to account for the possibility of several frequencies and forward and backward waves. It should be pointed out that an equation of the form (3) is self-evident when one deals with a two-level system, the lower level of which has a relaxation rate so fast that it is practically empty. When this is not the case, then, in general, one would have to set up two coupled integro-differential equations of the form (3).

Invoking the principle of detailed balance at equilibrium in the absence of a laser field, $n(v) = n_o(v)$, we obtain a relationship for the cross-relaxation rates:

$$\Gamma(v',v)\, n_o(v) = \Gamma(v,v')\, n_o(v').$$ (4)

It is convenient to define a symmetric function $\gamma(v,v')$ in terms of which both cross-relaxation rates can be expressed.

$$\gamma(v,v') = \gamma(v',v) \equiv \Gamma(v',v)\, n_o(v).$$ (5)

From (3) we find that in the steady-state equilibrium in the absence of an electric field the two integrals cancel and we find a relationship for the pump.

$$R(v) = \gamma(v)\, n_o(v).$$ (6)

This, in a sense, is the definition of the pump term in (3). Now consider the change $\Delta n(v)$ in the population inversion density $\Delta n(v) = n(v) - n_o(v)$. Taking the difference of (3) in the steady state $\left(\frac{\partial}{\partial t} = 0\right)$ in the presence of a laser field with its form in the absence of a laser field we obtain an equation for $\Delta n(v)$:

$$0 = -\gamma(v)\, \Delta n(v) - \int \frac{\gamma(v',v)}{n_o(v)}\, \Delta n(v)\, dv' + \int \frac{\gamma(v,v')}{n_o(v')}\, \Delta n(v')\, dv' - \frac{c}{8\pi}\sum_{k,\omega}\frac{2}{\hbar\omega}\, n(v)\, \sigma(v,k,\omega)\, E^2(k,\omega).$$ (7)

Equation 7 can be reduced to an equation in the variable $\Delta n(v)$ only if one makes an approximation that can be called the van der Pol approximation; namely, the assumption that the gain constant decreases linearly with optical intensity. In this assumption we replace $n(v)$ in (7) with the equilibrium inversion density $n_o(v)$.

$$0 = -\gamma(v)\, \Delta n(v) - \int \frac{\gamma(v',v)}{n_o(v)} \Delta n(v)\, dv' + \int \frac{\gamma(v,v')}{n_o(v')} \Delta n(v')\, dv'$$

$$- \frac{c}{8\pi} \sum \frac{2}{\hbar\omega} n_o(v)\, \sigma(v,k,\omega)\, E^2(k,\omega). \tag{8}$$

We can obtain a closed-form solution for (8) with one reasonable assumption for the relationship parameters. If we assume that $\gamma(v)$ is a constant, independent of v, and we set

$$\gamma(v,v') = \frac{1}{\tau} \frac{n_o(v)\, n_o(v')}{N_o}, \tag{9}$$

where

$$N_o = \int n_o(v)\, dv \tag{10}$$

and τ is a constant with the dimensions of time, and thus is a measure of the cross-relaxation time, we can show by direct substitution that

$$\Delta n(v) = -\frac{1}{\Gamma} \frac{c}{2h\omega} \sum_{k,\omega} n_o(v)\, \sigma(v,k,\omega)\, E^2(k,\omega) - \frac{1}{\Gamma\gamma\tau} n_o(v) \int \frac{n_o(v')}{N_o} dv' \sum_{k,\omega} \frac{c}{2h\omega} \sigma(v',k,\omega)\, E^2(k,\omega) \tag{11}$$

is a solution of (8), with

$$\Gamma = \gamma + \frac{1}{\tau}. \tag{12}$$

The solution (11) implies the existence of a hole burned by the laser field, and also a decrease in the population inversion density over the entire inhomogeneously broadened line.

Note that assumption (9) for the cross relaxation is eminently reasonable. The cross relaxation would be expected to be proportional to the two population densities participating in the cross relaxation, $n(v)\, n(v')$. If we assume that $n(v)$ deviates only slightly from the equilibrium density $n_o(v)$, and we expand to first order in $\Delta n(v)$, we obtain a rate equation for $\Delta n(v)$ with relaxation rates that obey (9).

We shall now apply the solution (11) to the analysis of the Lamb dip in a standing-wave cavity. Oscillation occurs when the loss L is equal to the gain within the medium. The loss is assumed, for simplicity, to be uniformly distributed over the cavity.

$$L = \int n_o(v)\left[\sigma(v, k, \omega) + \sigma(v, -k, \omega)\right] dv + \int \Delta n(v)\left[\sigma(v, k, \omega) + \sigma(v, -k, \omega)\right] dv. \tag{13}$$

In the sequel, we shall consider the limit in which the inhomogeneous broadening is very large compared with the homogeneous part. We shall assume that the cross section σ has the dependence upon the velocity:

$$\sigma = \frac{\sigma_o}{1 + \left[\omega - \omega_o\left(1 - \frac{k \cdot v}{|k|c}\right)\right]^2 T_2^2}. \tag{14}$$

This is the cross section originating from a Lorentzian line shifted by the Doppler effect.

When this expression is introduced into (11) and the integrals are carried out under the stated assumption, we obtain for $E^2(+k, \omega)$

$$E^2 = \sqrt{\frac{2}{\pi}} \frac{\Delta\omega T_2 2h\omega_o}{c\sigma_o^2 N_o} \Gamma \frac{G_o - Le^{\frac{(\omega-\omega_o)^2}{2\Delta\omega^2}}}{1 + \frac{1}{1 + (\omega-\omega_o)^2 T_2^2} + \frac{2\sqrt{2\pi}}{\gamma\tau\Delta\omega T_2}}, \tag{15}$$

where

$$G_o = \frac{2N_o\sigma_o\pi c}{u(2\pi)^{1/2}\omega_o T_2}. \tag{16}$$

Note that the output power P of the laser is related to E^2 by

$$P = \frac{c}{8\pi} E^2 A(1-R), \tag{17}$$

where A is the beam cross section, and R is the reflectivity of the mirror. We have assumed throughout that the field is uniform throughout the cavity, the usual assumption. Inclusion of the nonuniformity of the field does not change the shape of the Lamb dip.

Consider Eq. 15. The cross relaxation appears in this expression through addition of the term $\sqrt{2\pi}/(\gamma\tau\Delta\omega T_2)$ in the denominator. When this term is comparable to, or greater than, one, the Lamb dip is decreased. The question arises whether it is

consistent with the assumption that went into the derivation of (15) to allow this term to become large; we have assumed that the inhomogeneous broadening is large compared with the homogeneous one, that is, $\Delta\omega T_2 \gg 1$. Then, the factor can be made large only by making $\gamma\tau \ll 1$. Note that τ must be larger than T_2 because it is the time within which particles leave their velocity group, and T_2 contains the contributions to bandwidth of cross relaxation. Thus the only way the term could be large is by making γ sufficiently small. Hence, these systems will show a strong effect of cross relaxation on the Lamb dip for which the rate of decay γ to other levels is slow compared with the cross-relaxation rates, so slow that $\gamma\tau\Delta\omega T_2 \ll 1$, even though $\Delta\omega T_2 \gg 1$.

From a Lamb dip in which the power is measured as a function of cavity-frequency tuning we are not able to distinguish the effect of cross relaxation from that of the "soft" collisions as defined by Szöke and Javan.[2] Both lead to the same shape of the Lamb dip. It is possible to see such an effect from an observation of the small-signal gain profile in a laser medium at one frequency, if the medium is saturated by a laser signal of a different frequency, both frequencies having a common energy level in the medium. If cross relaxation is effective, the small-signal gain at one frequency would be affected by the saturating signal over the entire Doppler linewidth, whereas in the absence of cross relaxation the gain would be changed only over the homogeneous linewidth. An experiment by Hänsch and Toschek[6] could be interpreted as exhibiting such an effect in He-Ne. (It was not interpreted in this way by these authors.)

We are, at present, preparing experiments in He-Ne and in CO_2 to determine the importance of the cross-relaxation effect.

The authors gratefully acknowledge numerous helpful discussions with Professor Abraham Szöke.

H. A. Haus, P. W. Hoff

References

1. W. E. Lamb, Jr., "Theory of an Optical Maser," Phys. Rev. 134, A1429-A1450 (1969).

2. A. Szöke and A. Javan, "Effects of Collisions on Saturation Behavior of the 1. 15-μ Transition of Ne Studies with He-Ne Laser," Phys. Rev. 145, 137-147 (1966).

3. T. J. Bridges, Private communication, 1968.

4. C. Bordé and L. Henry, "Study of the Lamb Dip and of Rotational Competition in a Carbon Dioxide Laser," IEEE J. Quantum Electronics, Vol. QE-4, pp. 874-879, November 1968.

5. W. R. Bennett, Jr., "Hole Burning Effects in an He-Ne Optical Maser," Phys. Rev. 126, 580-593 (1962).

6. T. Hänsch and P. Toschek, "Observation of Saturation Peaks in He-Ne Laser by Tuned Laser Differential Spectrometry," IEEE J. Quantum Electronics, Vol. QE-4, pp. 467-468, July 1968.

B. SOLUTION OF WAVEGUIDE OBSTACLE PROBLEMS BY A FINITE-DIFFERENCE METHOD[*]

1. Introduction

This report describes a numerical method that has been used successfully for a digital computer calculation of the induced current distribution produced by a waveguide mode at a given frequency, impinging on metallic obstacles located inside a hollow metallic waveguide. The method was developed for the computer-aided determination of equivalent circuits for one or more passive metallic obstacles of irregular shape located inside a hollow metallic waveguide of arbitrary cross section.

The method is based on solving a set of finite difference equations which approximates Maxwell's equations, subject to field boundary conditions that approximate the exact field boundary conditions, in order to determine current distributions that approximate the exact induced current distributions. The approximation of Maxwell's equations by finite-difference equations was first achieved by Kron in order to simulate electromagnetic field problems on the General Electric Network Analyzer by means of electrical circuits.[1] In order to simulate electromagnetic field problems on a digital computer, a new set of finite-difference equations that approximates Maxwell's equations in free space was obtained; these equations were solved analytically for uniform and nonuniform plane waves.[2] This report extends the free-space difference equations to problems involving perfectly conducting boundaries and electric current distributions.

This report gives a general description of the technique, a discussion of TE_{m0} modes in rectangular waveguide which satisfy the difference equations, and a detailed formulation of TE_{m0} mode scattering. Numerical results on the accuracy of the calculations are given. Numerical results for the finite-length thin bifurcation and the computer time required for each calculation are also included.

2. Description of Problem and Technique

The waveguide obstacle problem consists in determining equivalent circuits or scattering matrices for highly conductive passive metallic obstacles located inside a hollow metallic waveguide. Well-known analytic variational and quasi-static techniques have been used successfully to solve special classes of obstacles exhibiting high degrees of symmetry.[3] The digital computer makes the finite-difference technique feasible for solving other classes of obstacles that may arise in microwave waveguide circuit design and have not been solved previously. This report is concerned with finding the induced

---

current on the obstacle's surface because the scattering matrix can be determined from the induced current.

An exact Green's function formulation of this boundary-value problem involves two integral equations. The first expresses the scattered fields in terms of the unknown distribution of induced current on the surface of the obstacles. The second expresses the fact that the electric field tangent to the surface of the obstacle exactly cancels the incident mode electric field distribution tangent to the obstacle. The finite-difference method proposed here is also a Green's function method and is best described in outline form.

1. Determine a finite set of waveguide modes.

   a. approximate Maxwell's equations by a set of difference equations for the field components evaluated at points of a cubic lattice.

   b. approximate the waveguide boundary by a series of points.

   c. solve the difference equations analytically or numerically to obtain a finite set of modes.

2. Determine the current-element field response of the waveguide.

   a. obtain fields produced at any point of the lattice by a discrete current element located at any point of the lattice as a superposition of modes.

3. Determine and solve algebraic equations for induced surface currents on the obstacle.

   a. approximate unknown induced surface current distribution by a set of discrete current elements located at lattice points.

   b. approximate the boundary condition that the total electric field (incident plus scattered) tangent to the obstacle vanish by the condition that the total field parallel to each discrete current element vanish.

   c. obtain scattered fields as a superposition of contributions from unknown current elements.

   d. from steps 3b and 3c obtain a set of simultaneous linear equation for the discrete current elements in terms of the incident mode electric field parallel to each current element.

   e. solve a set of equations by relaxation or Gauss-Jordan reduction to obtain discrete current-element values.

4. Determine the scattering matrix.

   a. obtain equations for forward- and backward-scattered mode amplitudes in terms of discrete current-element values from 3c.

   b. substitute discrete current-element values in Eq. 4c.

Each step in this procedure has been verified for related problems. The numerical calculation of modes for waveguides having irregular boundaries has been demonstrated.[4] The approximation of a continuous current distribution by discrete elements and the point-matching technique for boundary conditions have been used for free-space scattering problems.[5]

Practical limitations to the accuracy of the method are available computation time and storage capacity, since the accuracy will increase as more points per unit volume are taken. For a given waveguide and number of points per unit volume, the modes need only be computed once and stored on magnetic tape. The accuracy can be tested by increasing the number of points per unit volume and observing subsequent changes in the results.

3. TE_{m0} Modes in Rectangular Waveguide for Discrete Space

The TE_{m0} modes in perfectly conducting rectangular waveguide for discrete space will now be presented. The waveguide is shown in Fig. V-2. It consists of M unit cells in the x direction and N unit cells in the y direction. The unit cell size is indicated by a. The circles are E grid points previously defined.[2] The H grid points are not shown. The E grid points are as follows.

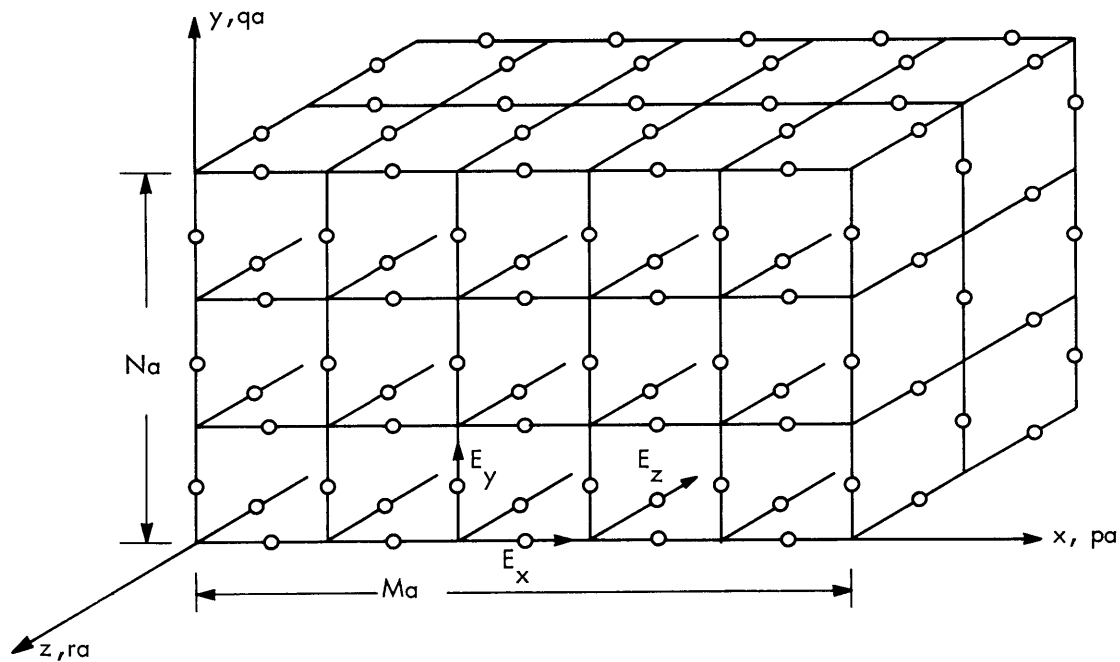Fig. V-2. E grid filling rectangular waveguide.

Electric Field	Lattice Point	Limits	
$E_x(p, q, r)$	$\left(p + \frac{1}{2}, q, r\right)$	$0 \leq p \leq M-1$	$0 \leq q \leq N$
$E_y(p, q, r)$	$\left(p, q + \frac{1}{2}, r\right)$	$0 \leq p \leq M$	$0 \leq q \leq N-1$
$E_z(p, q, r)$	$\left(p, q, r + \frac{1}{2}\right)$	$0 \leq p \leq M$	$0 \leq q \leq N$

where p, q, r are integers denoting the point (x, y, z) given by (pa, qa, ra), as shown in Fig. V-2. The H grid points are given by

Magnetic Field	Lattice Point	Limits	
$H_x(p, q, r)$	$\left(p, q + \frac{1}{2}, r + \frac{1}{2}\right)$	$0 \leq p \leq M$	$0 \leq q \leq N-1$
$H_y(p, q, r)$	$\left(p + \frac{1}{2}, q, r + \frac{1}{2}\right)$	$0 \leq p \leq N-1$	$0 \leq q \leq N$
$H_z(p, q, r)$	$\left(p + \frac{1}{2}, q + \frac{1}{2}, r\right)$	$0 \leq p \leq M-1$	$0 \leq q \leq N-1$

The electric current distribution will be given by discrete current densities located at the E grid points, J_x, J_y, and J_z.

Current Distribution	Lattice Point	Limits	
$J_x(p, q, r)$	$\left(p + \frac{1}{2}, q, r\right)$	$0 \leq p \leq M-1$	$1 \leq q \leq N-1$
$J_y(p, q, r)$	$\left(p, q + \frac{1}{2}, r\right)$	$1 \leq p \leq M-1$	$0 \leq q \leq N-1$
$J_z(p, q, r)$	$\left(p, q, r + \frac{1}{2}\right)$	$1 \leq p \leq M-1$	$1 \leq q \leq N-1$

Maxwell's equations including the current distribution can be approximated by the following difference equations.

$$E_z(q+1) - E_z(q) - E_y(r+1) + E_y(r) = -j\omega\mu_o a H_x(p, q, r) \tag{1}$$

$$E_x(r+1) - E_x(r) - E_z(p+1) + E_z(p) = -j\omega\mu_o a H_y(p, q, r) \tag{2}$$

$$E_y(p+1) - E_y(p) - E_x(q+1) + E_x(q) = -j\omega\mu_o a H_z(p, q, r) \tag{3}$$

$$H_z(q) - H_z(q-1) - H_y(r) + H_y(r-1) = a(j\omega\epsilon_o E_x(p, q, r) + J_x(p, q, r)) \tag{4}$$

$$H_x(r) - H_x(r-1) - H_z(p) + H_z(p-1) = a(j\omega\epsilon_o E_y(p, q, r) + J_y(p, q, r)) \tag{5}$$

$$H_y(p) - H_y(p-1) - H_x(q) + H_x(q-1) = a(j\omega\epsilon_0 E_z(p, q, r) + J_z(p, q, r)) \tag{6}$$

The modes are obtained by looking for current-free solutions of the previous equations which vary with r as e^{-rw}, where w is a complex number, and satisfy the boundary conditions at the perfectly conducting walls.

$$E_x = 0 \qquad \text{for } q = 0 \text{ and } q = N$$

$$E_y = 0 \qquad \text{for } p = 0 \text{ and } p = M$$

$$E_z = 0 \qquad \text{for } p = 0, \ q = 0, \ q = N, \text{ and } p = M.$$

It can be shown that there are $(M-1)(N-1)$ TM modes and $(MN-1)$ TE modes whose field components vary as e^{-rw}, where w is given by

$$w = \pm j2 \ \sin^{-1} \left(\sqrt{(ka/2)^2 - \sin^2 \ (s\pi/2M) - \sin^2 \ (t\pi/2N)} \ \right). \tag{7}$$

Here, k is the propagation constant of free space, and s and t are integers. For TE modes that do not vary along y simple expressions for the field components can be obtained.

$$\underline{TE_{s0} \text{ Modes}}$$

$$E_y = B \sin (ps\pi/M) \ e^{-rw(s)} \qquad\qquad 0 \leqslant p \leqslant M \tag{8}$$

$$H_x = -(B/j\omega\mu_0 a)(1-e^{-w}) \sin (ps\pi/M) \ e^{-rw(s)} \qquad 0 \leqslant p \leqslant M-1 \tag{9}$$

$$H_z = -(B/j\omega\mu_0 a) \cdot 2 \sin (s\pi/2M) \cos \left(\left(p + \tfrac{1}{2}\right) s\pi/M \right) e^{-rw(s)} \quad 0 \leqslant p \leqslant M-1. \tag{10}$$

The subscript "s" is used instead of "m" to distinguish these modes from the exact TE_{m0} modes in rectangular waveguide; s is an integer and $w(s)$ is given by

$$w(s) = \pm j2 \ \sin^{-1} \left(\sqrt{(ka/2)^2 - \sin^2 \ (s\pi/2M)} \right) \qquad 1 \leqslant s \leqslant M-1. \tag{11}$$

Figure V-3 shows the E_y field for the TE_{10} and TE_{20} modes for different numbers of cells. The cutoff frequencies for the modes are given by setting $w = 0$

$$f_{c.o.} = (c/\pi a) \sin (s\pi/2M) \quad \text{Hz,} \tag{12}$$

where c is the speed of light in vacuum. In Fig. V-4 the normalized cutoff frequencies

TE₁₀ MODE

TE₂₀ MODE
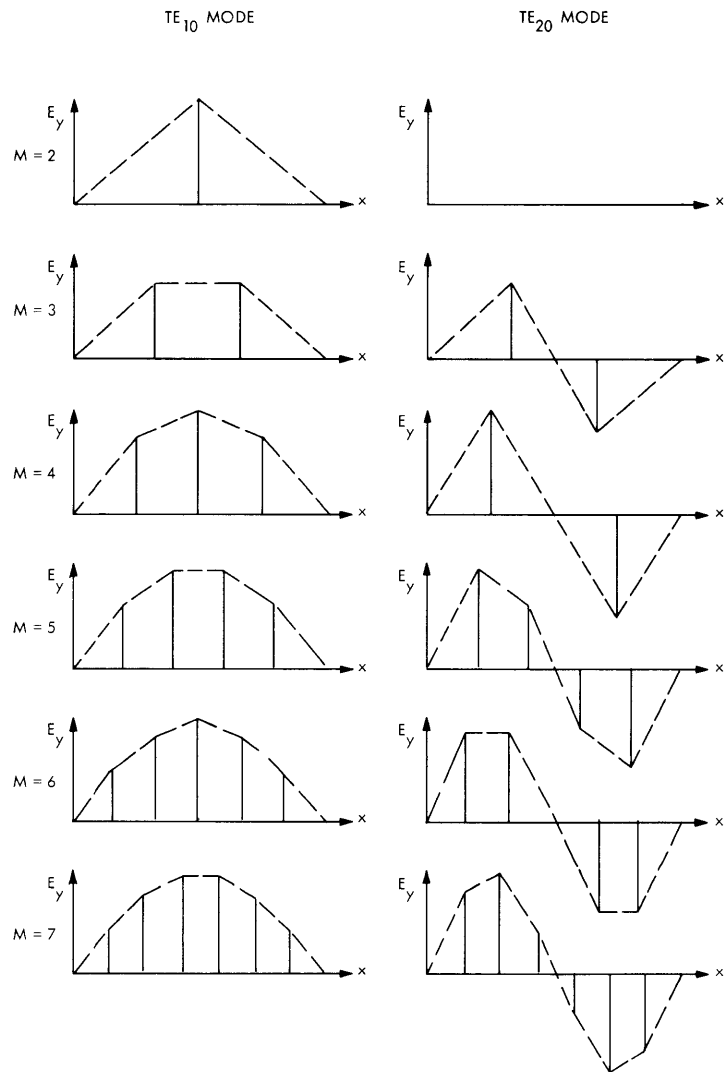
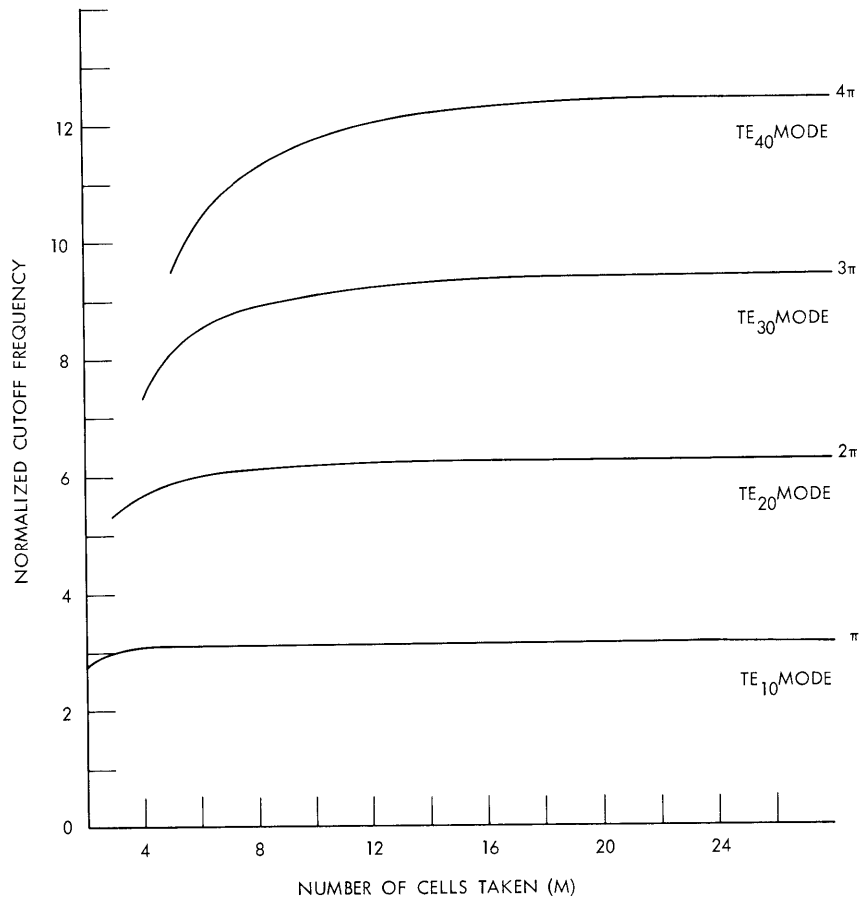Fig. V-3. E_y field for TE₁₀ and TE₂₀ modes; M = 2, 3, 4, 5, 6, 7.

Fig. V-4.   Cutoff frequencies of TE_{m0} modes of rectangular
waveguide vs number of cells.

for several modes have been plotted against the number of cells taken.   The limiting
values are the normalized cutoff frequencies for an infinite number of cells.

The TE_{s0} modes also obey a completeness condition that can be written

$$\delta_{pp_0} = (2/M) \sum_{s=1}^{s=M-1} \sin(ps\pi/M) \sin(p_0 s\pi/M),$$ (13)

where δ denotes a Kronecker delta function.   This condition will be used to determine
the Green's function for the discrete waveguide, excited by y-directed currents that do
not vary with y.

4.   Green's Function for TE_{s0} Modes

The Green's function for the TE_{s0} modes will now be obtained.   The Green's func-
tion is defined as the solution of Eqs. 1-6, subject to the boundary conditions at the
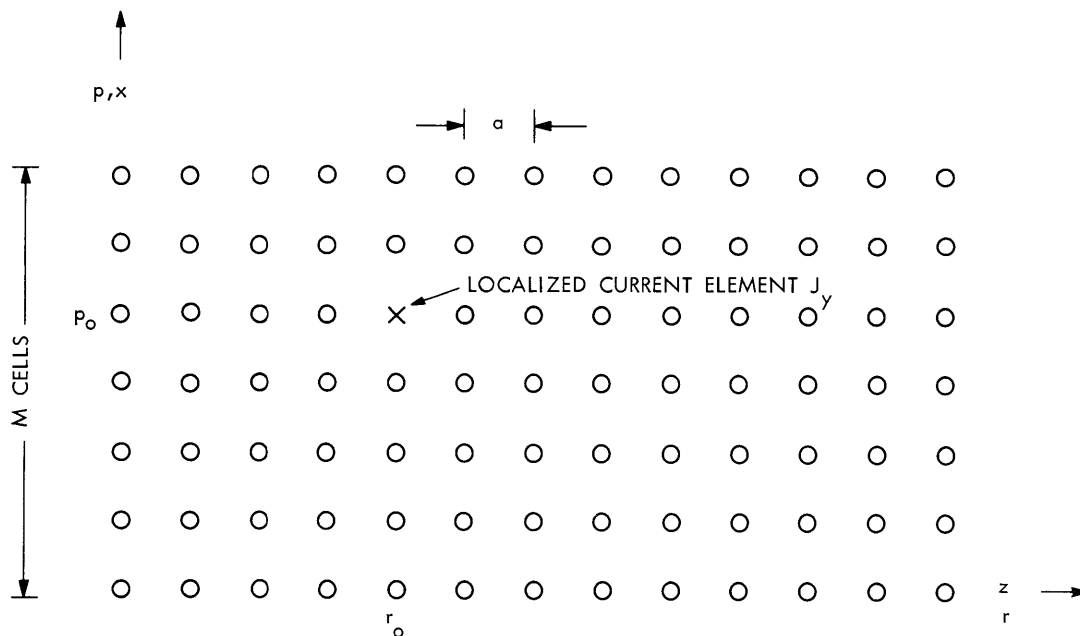
Fig. V-5. Two-dimensional view of E grid with current element.

waveguide walls, for a current distribution that is zero except at one point; in general there will be a Green's function for each current component. For the case of y-directed currents that do not vary with y, a simple Green's function in two dimensions, x and z, can be found as a superposition of TE_{s0} modes. This result will be used to determine the fields produced when a TE_{s0} mode impinges on a perfectly conducting two-dimensional obstacle extending across the rectangular waveguide. Numerical results on the self-impedance of the current element will be given.

A two-dimensional view of the lattice is given in Fig. V-5. The current is located at point p_o, r_o and is given by

$$J_y(p, q, r) = (I/a^2) \, \delta_{rr_o} \delta_{pp_o} \qquad A/m^2, \qquad (14)$$

where δ is the Kronecker delta function, and I is a constant. The Green's function is obtained by solving Eqs. 1-6 for the fields generated by J_y. The completeness condition (Eq. 13) shows that the current distribution given by Eq. 14 is a superposition of orthogonal transverse current distributions, each varying with p as the E_y field of a TE_{s0} mode.

The result is that only TE_{s0} modes are generated for $r > r_o$ and for $r < r_o$, and the total electric field is given by the following series.

$$E_y(p, q, r) = \left(\frac{-j\omega\mu_o I}{2}\right)\left(\frac{2}{M}\right) \sum_{s=1}^{s=M-1} \frac{\sin(ps\pi/M)\sin(p_o s\pi/M)}{\sinh(w)} e^{-|r-r_o|w}. \qquad (15)$$

It is convenient to define the normalized Green's function $Z'(p, r, p_0, r_0)$, where

$$Z'(p, r, p_0, r_0) = (E_y/I) \qquad \Omega/m. \tag{16}$$

Z' is the electric field produced at point (p, r) by a unit current element located at point (p_0, r_0).
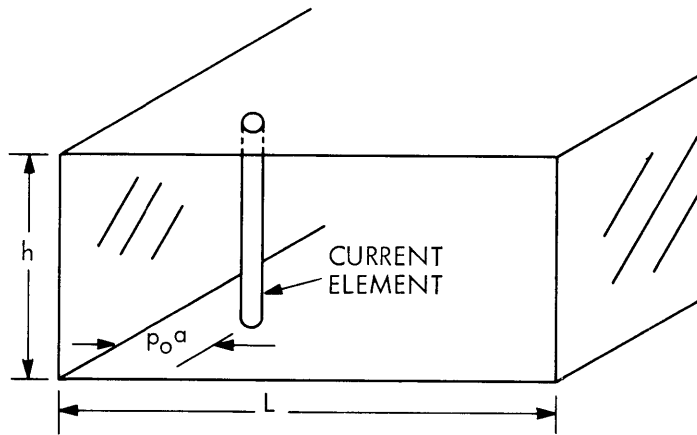

Fig. V-6. Perspective view of current element in rectangular waveguide.

The self-impedance of a unit current element located in a rectangular waveguide as shown in Fig. V-6 has been computed for several different numbers of cells as a function of position across the waveguide. The self-impedance is defined as Z_s, where

$$Z_s = Z'(p_0, r_0, p_0, r_0) \cdot h \qquad \Omega, \tag{17}$$

and h is the height of the waveguide. The real and imaginary parts of Z_s normalized to Z_0, the characteristic impedance of free space, are shown in Figs. V-7 and V-8. The parameters have been chosen so that one mode is above cutoff: L = 2.54 cm, h = 1.00 cm, f = 9.0 GHz. The real part of Z_s, which is proportional to the radiated power, is well approximated for small M. The imaginary part, which is approximately proportional to the magnetic energy storage, diverges with M logarithmically as the current element more and more closely approximates a line source; the shape converges rapidly to a smooth function. Z_s has been computed for the same waveguide for a frequency of 72 GHz and M = 100; the real and imaginary parts appear in Figs. V-9 and V-10; at 72 GHz 12 modes are above cutoff.

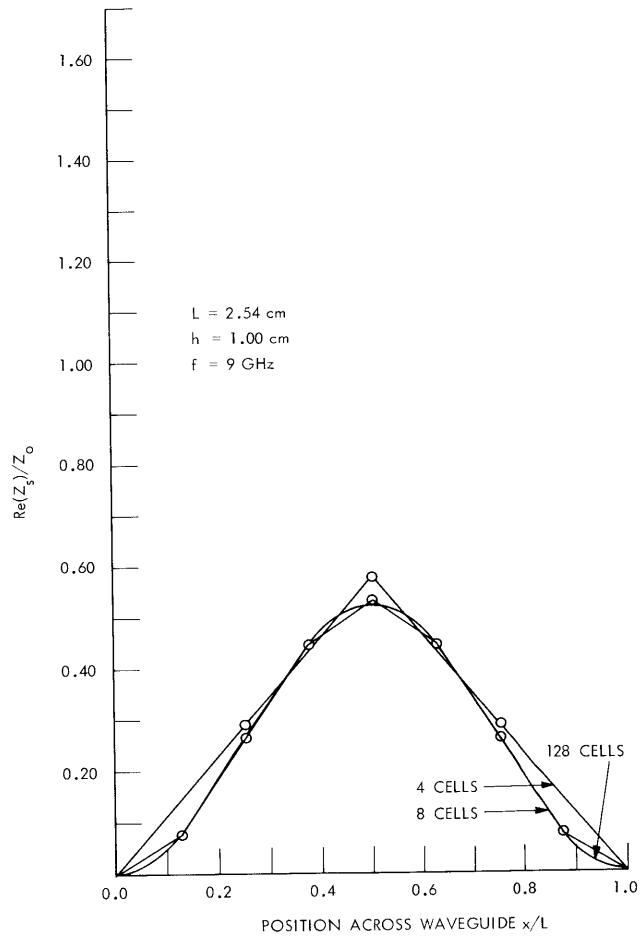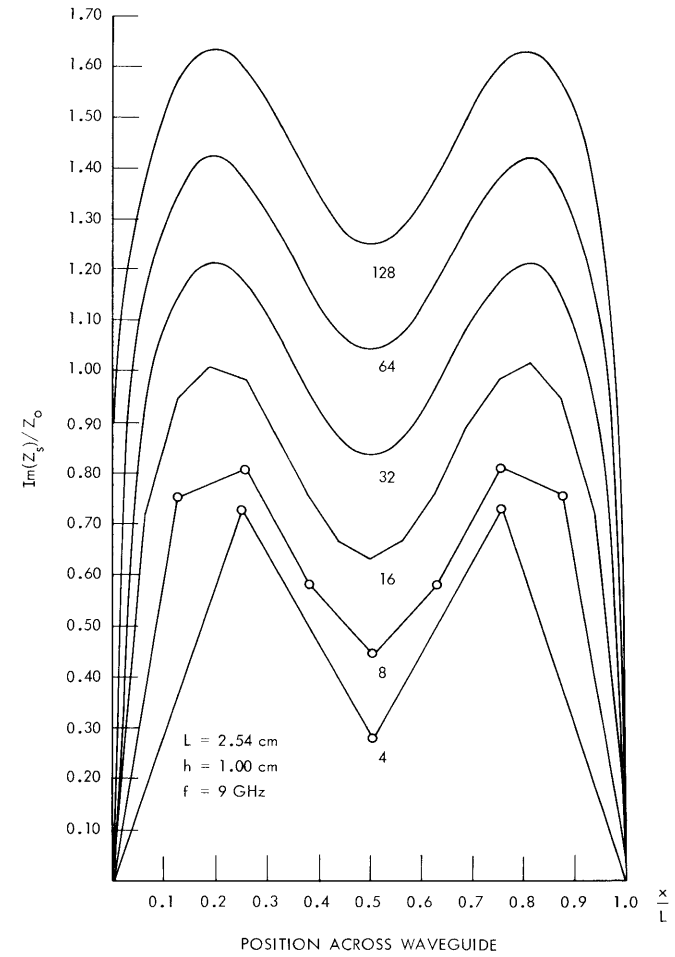Fig. V-7. Normalized real part of Z_s vs position for $M = 4, 8, 128$, $f = 9$ GHz.

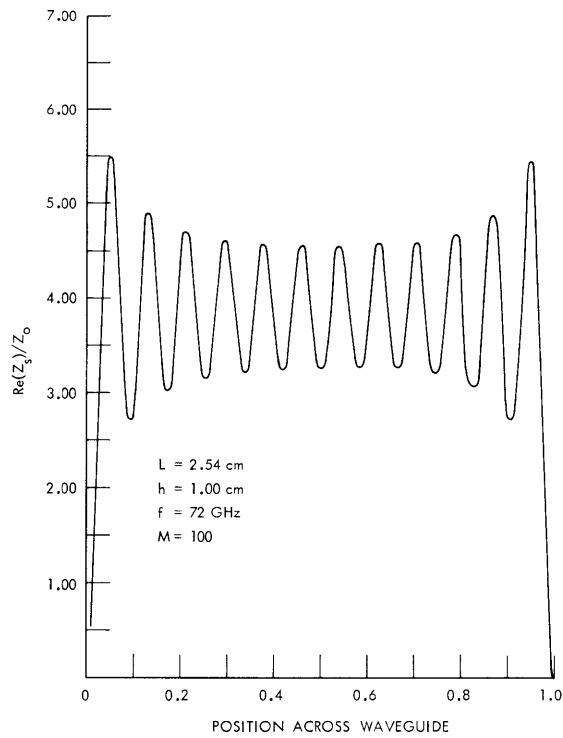Fig. V-8. Normalized imaginary part of Z_s vs position for $M = 4, 8, 16, 32, 64, 128$, $f = 9$ GHz.

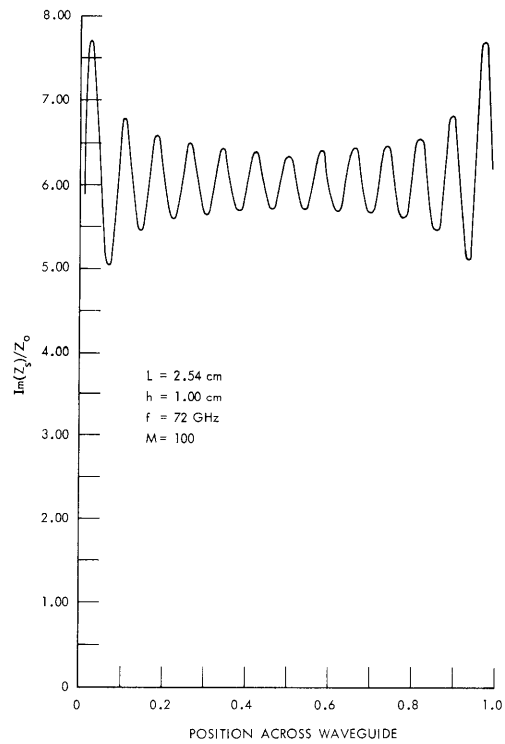Fig. V-9.   Normalized real part of Z_s vs position for
M = 100, f = 72 Ghz.

Fig. V-10.   Normalized imaginary part of Z_s vs position for
M = 100, f = 72 Ghz.

5.   Scattering of TE_{s0} Waves by Two-Dimensional Obstacles

The Green's function that has been obtained will be used to formulate and solve the problem of TE_{s0} modes impinging on two-dimensional metallic obstacles of arbitrary shape.   The results will be used to obtain the induced current distribution on the surface of the obstacle.   Numerical results for the thin finite-length bifurcation will be presented eventually.

The incident field in the TE wave is given by

$$\overline{E} = \overline{i}_y e(x, z). \tag{18}$$

The problem is formulated in two steps.   In the first step, the actual current distribution is approximated by a discrete current distribution, which consists in y-directed current elements lying at E_y points near the contour of the body.   For the case shown in Fig. V-11 the induced current distribution is approximated by 20 currents.   In the second
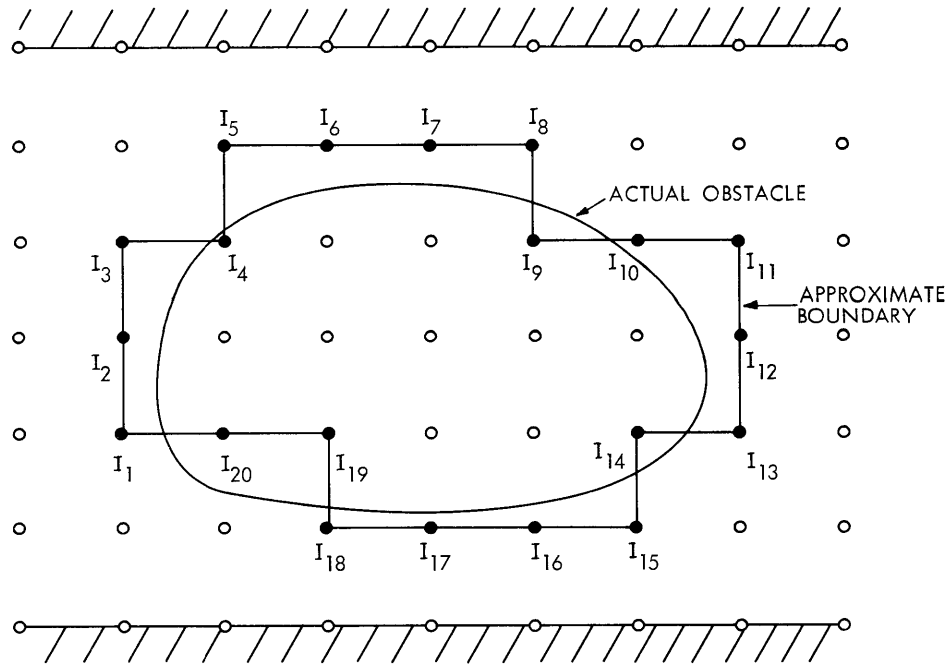

Fig. V-11.   Two-dimensional view of obstacle approximated
by current elements.

step, the boundary condition that the tangential electric field vanish will be applied to each current element in order to relate the E_y field at a point to each induced current.

The boundary points will be labeled by the index n so that

$$p_n = p(n) \qquad n = 1, 2, 3\dots$$
$$r_n = r(n) \qquad n = 1, 2, 3\dots$$

(19)

and the discrete currents will be denoted I_n. The incident field evaluated at the boundary points will be taken as

$$E_y(n) = e(p_n, r_n) = e(n).$$

(20)

The total E_y field produced by the currents $I_1, I_2 \dots$ at point (p, r) is given by a sum of terms similar to Eq. 15.

$$E_y(p, r) = \sum_n Z'(p, r, p_n, r_n)\, I_n.$$

(21)

The boundary condition that the total electric field vanish at each current element is then given by

$$e(n) + E_y(p_n, r_n) = 0 \quad \text{for all n.}$$

(22)

Equation 22 gives rise to a set of simultaneous linear equations for the I_n

$$e(n) + \sum_{n'} Z'(p_n, r_n, p'_n, r'_n)\, I'_n = 0.$$

(23)

Equation 23 can be written as a matrix equation

$$e + \underline{Z}'I = 0,$$

(24)

where I is a column vector containing the I_n, e is a column vector containing the $e(n)$, and $\underline{Z}'$ is a square matrix whose order equals the number of current elements. The elements of $\underline{Z}'$ are given by $\underline{Z}'(n, n')$, where

$$\underline{Z}'(n, n') = \left(\frac{-j\omega\mu_o}{2}\right)\left(\frac{2}{M}\right) \sum_{s=1}^{M-1} \frac{\sin\,(p_n s\pi/M)\,\sin\,(p'_n s\pi/M)}{\sinh\,(w(s))}\, e^{-\left|r_n - r'_n\right|w}.$$

(25)

Z' is the mutual coupling matrix between all of the current elements. The diagonal terms are the self-impedances previously computed, and the matrix is symmetrical. Inversion of Eq. 24 constitutes the solution to the problem. The scattering into the various modes

can be determined from the following definition of the scattering coefficient into the sth mode, S_s.

$$E_y(p, r) = \sum_{s=1}^{M-1} S_s(r) \sin (ps\pi/M). \tag{26}$$

S_s is given by

$$S_s(r) = \left(\frac{-j\omega\mu_o}{2}\right) \left(\frac{2}{M}\right) \sum_n \frac{\sin (p_n s\pi/M)}{\sinh (w(s))} I_n\, e^{-\left|r-r_n\right| w(s)}. \tag{27}$$

6. Numerical Results for Thin Finite-Length Bifurcation

Equation 24 was solved numerically for the TE_{10} mode impinging upon a thin finite-length bifurcation located in the center of the rectangular waveguide as shown in Fig. V-12. The waveguide parameters were L = 2.54 cm, h = 1.00 cm, f = 9.00 GHz,
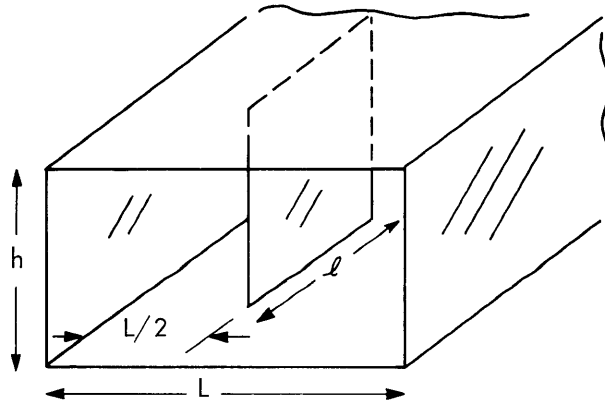

Fig. V-12. Perspective view of thin finite-length bifurcation.

M = 100. Each element of the $\underline{Z}'$ matrix above and on the main diagonal was computed, although the symmetry of the obstacle could have been used to reduce the number of different terms drastically. The elements below the main diagonal were not computed, since $\underline{Z}'$ is symmetrical. Gauss-Jordan reduction was used to solve the resulting equations. As a check on the roundoff error, the resulting current elements were used in Eq. 24 to recompute the scattered field.

The current distribution was obtained for bifurcations of lengths ℓ = 0.254, 0.508, 0.762, and 1.016 cm, consisting of 10, 20, 30, and 40 current elements, respectively;
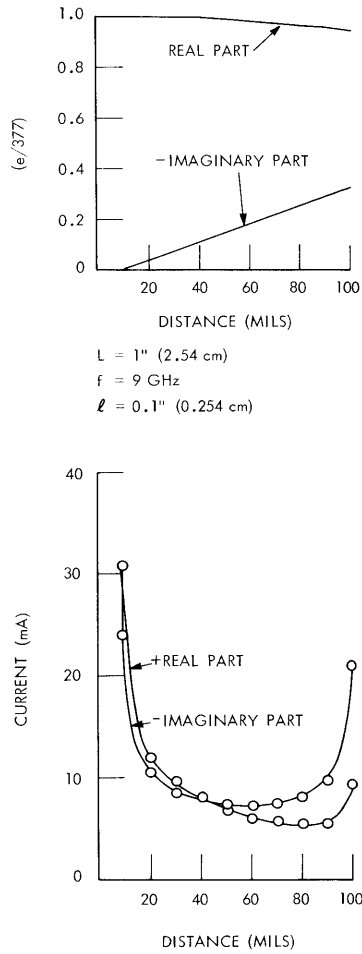
Fig. V-13. Induced current distribution on 10-element bifurcation excited by the TE_{10} mode.
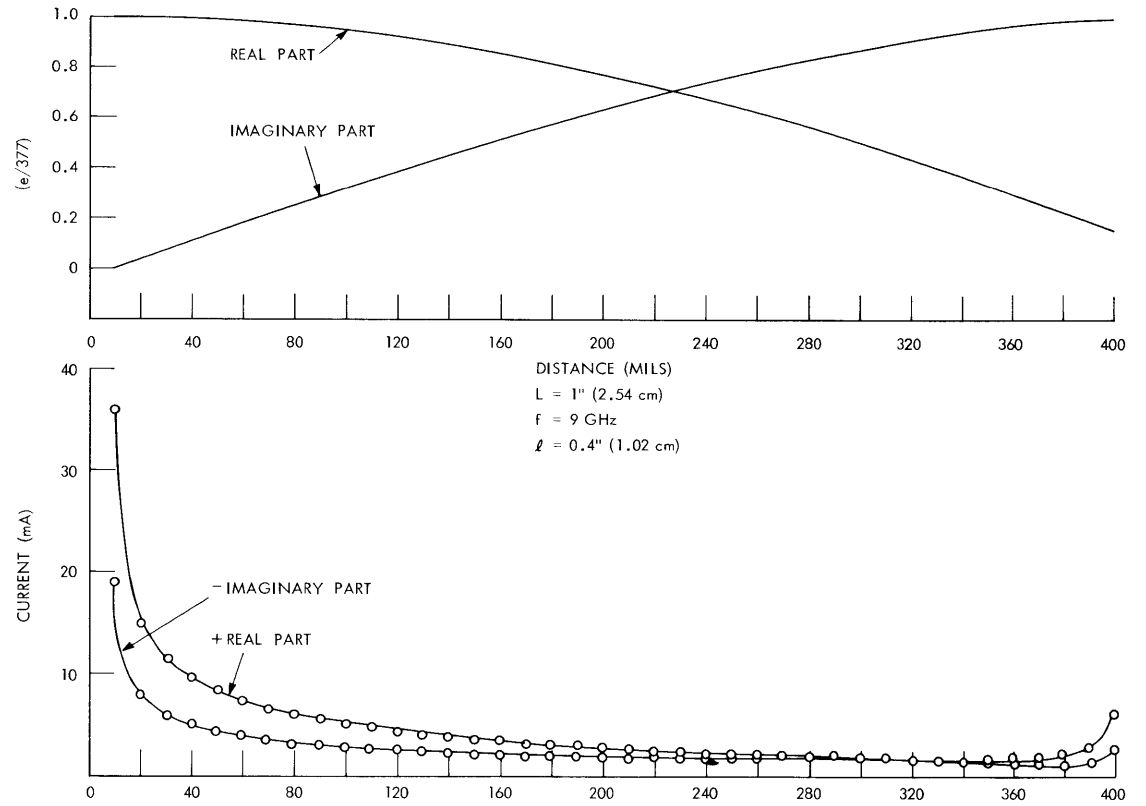

Fig. V-14. Induced current distribution on 40-element bifurcation excited by the TE_{10} mode.

the 10 and 40 element cases are shown in Figs. V-13 and V-14. The incident electric field was 377 V/m at the center of the waveguide, and the normalized electric field is plotted above the current distribution curve. The computation time and roundoff error in parts per million are plotted in Fig. V-15 as a function of the number of current elements. The IBM 360/65 computer was used.
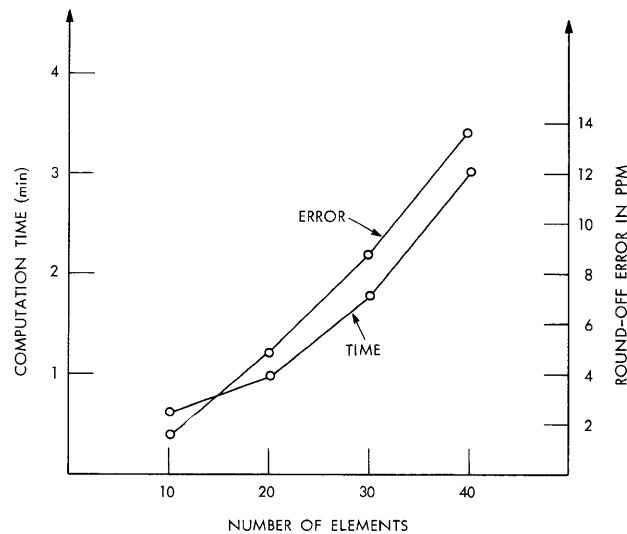

Fig. V-15. Computation time and roundoff error vs number of current elements.

7. Conclusion

In principle, the method can be extended to the case of a three-dimensional obstacle. This involves computation of a Green's dyadic function consisting of a sum of TE and TM modes. In practice, the time for computing the Green's function will not be prohibitive; however, the time for inverting the mutual coupling matrix for even simple obstacles may exceed 10 minutes. The roundoff error may become prohibitive unless double-precision arithmetic is used; for example, an error of 4 parts in 10^5 was found for 99 current elements.

J. I. Glaser

References

1. G. Kron, "Equivalent Circuit of the Field Equations of Maxwell — I," Proc. IRE 32, 289-299 (1944).

2. J. I. Glaser, "Maxwell's Equations for Discrete Space," Quarterly Progress Report No. 92, Research Laboratory of Electronics, M. I. T., January 15, 1969, pp. 211-219.

3. N. Marcuvitz, <u>Waveguide Handbook</u>, Radiation Laboratory Series Vol. 10 (McGraw-Hill Book Company, New York, 1948).

4. J. B. Davies and C. A. Muilwyk, "Numerical Solution of Hollow Waveguides with Boundaries of Arbitrary Shape," Proc. IEEE <u>113</u>, 277-288 (1966).

5. R. L. Tanner and M. G. Andreasen, "Numerical Solution of Electromagnetic Problems," IEEE Spectrum, Vol. 4, No. 9, pp. 53-61, 1968.